Available online at www.sciencedirect.com

ScienceDirect

Procedia IUTAM 22 (2017) 146 – 153

Procedia IUTAM

www.elsevier.com/locate/procedia

IUTAM Symposium on Nonlinear and Delayed Dynamics of Mechatronic Systems

Influence of Workpiece Imbalance on Regenerative and Frictional Grinding Chatters

Yao Yan[a,*], Jian Xu[b], Marian Wiercigroch[c]

[a]School of Aeronautics and Astronautics, University of Electronic Science and Technology of China, 2006 Xiyuan Road, Chengdu 611731, China
[b]School of Aerospace Engineering and Applied Mechanics, Tongji University, 1239 Siping Road, Shanghai 200092, China
[c]Centre for Applied Dynamics Research, School of Engineering, University of Aberdeen, Fraser Noble Building, King's College, Aberdeen AB24 3UE, UK

Abstract

This paper investigates regenerative and frictional grinding chatters affected by mass eccentricity in the workpiece. Time delays and velocity-soften friction coefficient are employed to represent regenerative and Stribeck effects in normal and tangential grinding forces. Eigenvalue calculation and continuation scheme are used to find stability boundaries for both regenerative and frictional instabilities, illustrating that a deep grinding enhances the regenerative stability but impairs the frictional one. Near each kind of boundaries, numerical simulations and bifurcation analyses are adopted to present various chatter motions in the grinding, either with or without mass eccentricity. It is found that the frictional chatter is prone to be quenched by the external excitation due to the mass eccentricity. On the contrary, the regenerative instability still persists, but is perturbed to be quasi-periodic.

Peer-review under responsibility of organizing committee of the IUTAM Symposium on Nonlinear and Delayed Dynamics of Mechatronic Systems

Keywords: Regenerative grinding chatter; Frictional chatter; Coulomb Stribeck; Workpiece Imbalance;

1. Description of the plunge grinding process

A typical plunge grinding process[1] is depicted in Fig. 1(a). With its end ($S = L$) simply supported by a tailstock, a workpiece has its head ($S = 0$) clamped and rotated by a chuck with an angular speed Ω_w [rad/s]. In the middle of the workpiece ($S = P$), a disc is lumped to be processed. On the right of the workpiece, a rotating grinding wheel is mounted on a wheel holder which moves along a horizontal guide, with an angular speed Ω_g [rad/s] and a feed speed f [m s^{-1}]. The workpiece has mass density ρ [kg m^{-3}], Young's modulus E [Mp], lateral damping c_w [N s m^{-2}], torsional viscous damping c_t [N s m rad^{-1}], radius R_w [m] and length L [m]. The disc is of mass m_d [kg], moment of inertia J_d [kg m^2], mass eccentricity e_d [m], width W [m] and radius R_d [m]. The mass of the grinding wheel is m_g [kg], and its equivalent stiffness and damping of the massless holder are k_g [N m^{-1}] and c_g [N s m^{-1}], respectively[2].

* Corresponding author.
E-mail address: y.yan@uestc.edu.cn

Peer-review under responsibility of organizing committee of the IUTAM Symposium on Nonlinear and Delayed Dynamics of Mechatronic Systems
doi:10.1016/j.piutam.2017.08.019

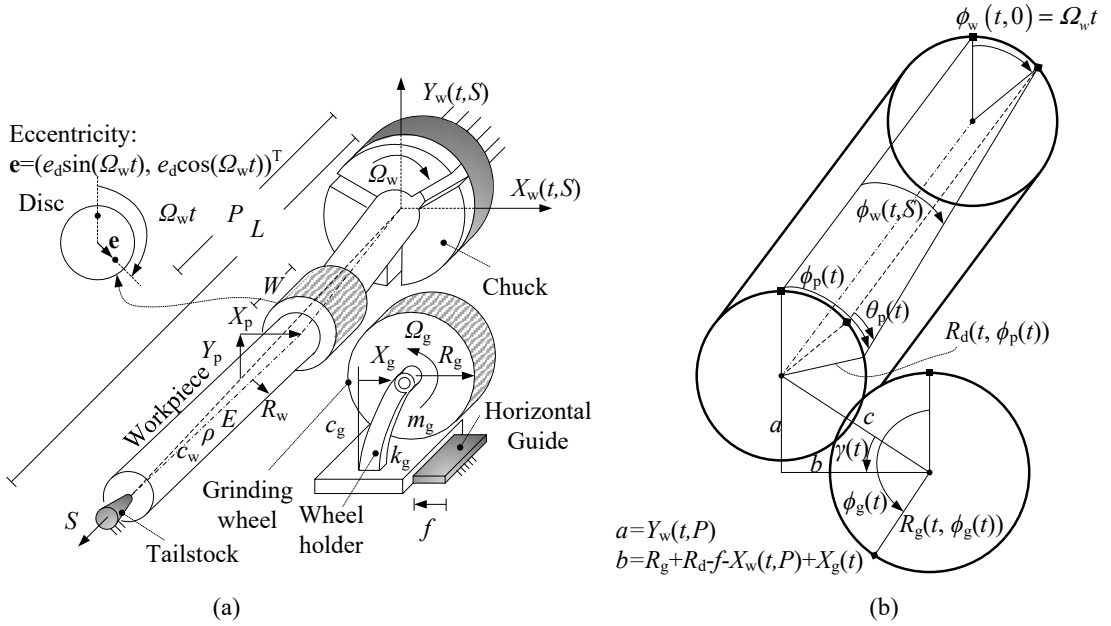

Fig. 1. (a) Schematic of the regenerative grinding process with mass eccentricity in the workpiece; (b) wheel-workpiece contact angle $\gamma(t)$ introduced by vertical workpiece displacement.

Under interactive grinding forces, the workpiece bends both horizontally ($X_w(t,S)$ [m]) and vertically ($Y_w(t,S)$ [m]), while the wheel holder yield a horizontal displacement ($X_g(t)$ [m]). Torsional movement of the workpiece is represented by $\phi_w(t,S)$. Driven by the chuck, the workpiece has $\phi_w(t,0) = \Omega_w t$. Denoting $\phi_p(t) = \phi_w(t,P)$, one can use $\theta_p(t) = \phi_p(t) - \phi_w(t,0)$ to describe the torsional workpiece motion. Due to the vertical workpiece motion, as seen in Fig. 1(b), the wheel-workpiece contact angle is

$$\gamma = \tan^{-1}\left(\frac{a}{b}\right) = \tan^{-1}\left(\frac{Y_w(t,P)}{R_g + R_d - f - X_w(t,P) + X_g(t)}\right). \tag{1}$$

Given the complex boundary conditions, the spatial-temporal continuum workpiece is discretized to yield the governing equation of the grinding process[2]:

$$\begin{aligned}
m_g\ddot{X}_g(t) + c_g\dot{X}_g(t) + k_g X_g(t) &= F_x(t),\\
m_w\ddot{X}_p(t) + c_w\dot{X}_p(t) + k_w X_p(t) &= -F_x(t) + 2m_d e_d\left(\dot{\phi}_p(t)\right)^2\sin\left(\phi_p(t)\right) - 2m_d e_d\ddot{\phi}_p(t)\cos\left(\phi_p(t)\right),\\
m_w\ddot{Y}_p(t) + c_w\dot{Y}_p(t) + k_w Y_p(t) &= F_y(t) + 2m_d e_d\left(\dot{\phi}_p(t)\right)^2\cos\left(\phi_p(t)\right) - 2m_d e_d\ddot{\phi}_p(t)\sin\left(\phi_p(t)\right),\\
J_t\ddot{\theta}_p(t) + c_t\dot{\theta}_p(t) + k_t\theta_p(t) &= c_t\Omega_w + M(t) - 2m_d e_d\ddot{X}_p(t)\cos(\phi) - 2m_d e_d\ddot{Y}_p(t)\sin(\phi).
\end{aligned} \tag{2}$$

where m_w, c_w, k_w, J_t, c_t, k_t are equivalent mass, lateral damping, stiffness, moment of inertia, torsional damping and torsional stiffness of the workpiece, respectively. Here, an overdot indicates a derivative with respect to time t.

It should be remarked that the contact angle γ is introduced by the vertical workpiece motion. When only the horizontal displacement is considered, which means the tangential frictional force and the workpiece imbalance do not play a role and thus the workpiece does not bend vertically, the model is degenerated to that studied in Ref.[3]. Such a model cannot be used to discuss the influences of wheel-workpiece friction and mass eccentricity on the grinding dynamics. More comparison between the regenerative and frictional instabilities can be found in Ref.[2].

The interactive wheel-workpiece grinding forces in Eq. (2), $F_x(t)$, $F_y(t)$ and $M(t)$, are displayed in Fig. 2. In terms of normal cutting force $F_n(t)$ and tangential frictional force $F_t(t)$, they are given by

$$\begin{aligned}
F_x(t) &= F_n(t)\cos(\gamma(t)) + F_t(t)\sin(\gamma(t)),\\
F_y(t) &= F_n(t)\sin(\gamma(t)) - F_t(t)\cos(\gamma(t)),\\
M(t) &= F_t(t)R_d.
\end{aligned} \tag{3}$$

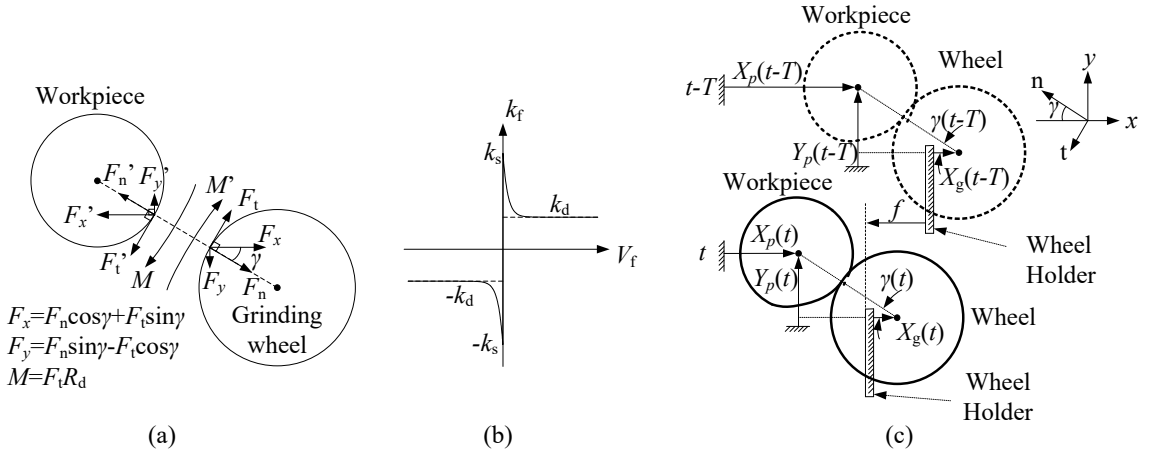

Fig. 2. (a) Grinding forces between the wheel and the workpiece; (b) Coulomb frictional coefficient with Stribeck effect; (c) Regenerative grinding depth.

When a loss of wheel-workpiece contact occurs (negative grinding depth $D_g < 0$), there are no interactive forces ($F_n = F_t = 0$). For a cutting ($D_g \geq 0$), they are proportional to the grinding depth[2]:

$$\begin{aligned} F_n(t) &= k_\mu \left(\frac{\Omega_w+\dot{\theta}_p-\dot{\gamma}}{\Omega_g+\dot{\gamma}}\right)^{2\mu-1} D_g^\mu, \\ F_t(t) &= k_f(V_f)F_n(t), \end{aligned} \tag{4}$$

where k_μ [N m$^{-\mu}$] is grinding stiffness, μ a dimensionless coefficient, k_f the frictional coefficient of the frictional velocity ,V_f.

In addition to the regenerative effect, the Stribeck effect in the tangential force is represented by the frictional coefficient displayed in Fig. 2(b), which is

$$\begin{aligned} k_f(V_f) &= \mathrm{sign}(V_f)\left(k_d + (k_s - k_d)\exp\left(-\tfrac{|V_f|}{V_s}\right)\right), \\ V_f &= \Omega_g R_g - \Omega_w R_w - \dot{\theta}_p(t)R_d + \dot{Y}_p(t)\cos(\gamma(t)) - \left(\dot{X}_g(t) - \dot{X}_p(t)\right)\sin(\gamma(t)), \end{aligned} \tag{5}$$

where $\mathrm{sign}(V_f)$ is the sign function of V_f, $|V_f|$ the absolute value of V_f, k_d the dynamic frictional coefficient, k_s the static frictional coefficient and V_s the dimensionless Stribeck friction velocity, respectively[6].

The grinding depth is represented by regenerative theory, which represents the instantaneous chip thickness by current and previous tool displacement[7]. According to the doubly regenerative theory[2,5,8,9], as seen in Fig. 2(c), the instantaneous grinding depth is represented by

$$\begin{aligned} D_g(t) = {} & f\cos(\gamma(t)) + X_p(t)\cos(\gamma(t)) - X_g(t)\cos(\gamma(t)) - Y_p(t)\sin(\gamma(t)) \\ & - X_p(t-T_w)\cos(\gamma(t-T_w)) + X_g(t-T_w)\cos(\gamma(t-T_w)) + Y_p(t-T_w)\sin(\gamma(t-T_w)) \\ & - gX_p(t-T_g)\cos(\gamma(t-T_g)) + gX_g(t-T_g)\cos(\gamma(t-T_g)) + gY_p(t-T_g)\sin(\gamma(t-T_g)), \end{aligned} \tag{6}$$

where $T_w = 2\pi/\Omega_w$ and $T_g = 2\pi/\Omega_g$ are rotational periods of the workpiece and the wheel and g is a small dimensionless parameter representing a comparatively slow regenerative speed of the wheel. Here, g depends on the grinding ratio $G_r = V_w/V_g$, where V_w is the volume of workpiece material removed and V_g the corresponding volume of the wheel[13]. According to Ref. [14], one has

$$g = \frac{\Omega_w R_d}{G_r \Omega_g R_g}. \tag{7}$$

Due to the vertical and torsional motions of the workpiece ($\gamma(t) \neq 0$ and $\theta_p(t) \neq 0$), T_w and T_g become state-dependent[10,11,12] and implicitly governed by

$$\begin{aligned} 2\pi &= \phi_p(t) - \gamma(t) - \phi_p(t-T_w) + \gamma(t-T_w) \\ &= \theta_p(t) - \gamma(t) - \theta_p(t-T_w) + \gamma(t-T_w) + T_w\Omega_w, \\ 2\pi &= \gamma(t) - \gamma(t-T_g) + T_g\Omega_g. \end{aligned} \tag{8}$$

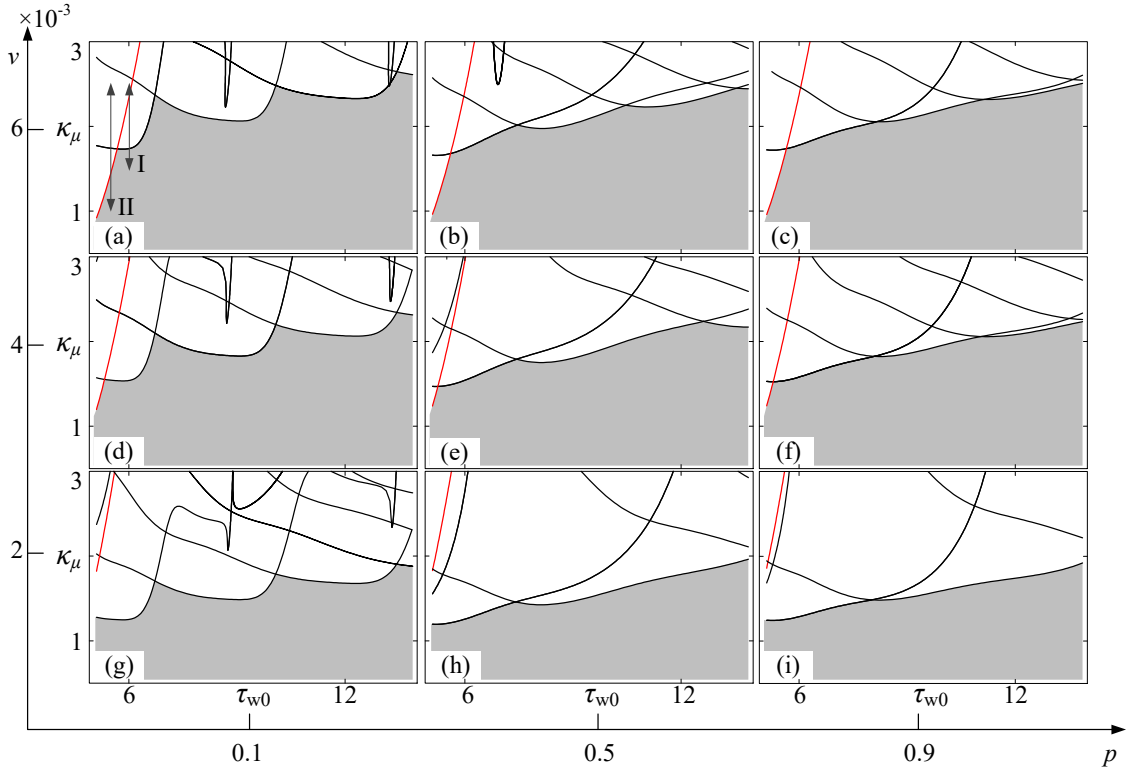

Fig. 3. Stability boundaries of the grinding process. For selected values of p (0.1, 0.5 and 0.9) and ν (0.002, 0.004 and 0.006), boundaries for regenerative (black) and frictional (red) instabilities are displayed in $\tau_{w0} - \kappa_\mu$ plane. Arrows I ($\tau_{w0} = 6.0$ and $\kappa_\mu \in [1.5, 2.5]$) and II ($\tau_{w0} = 5.5$ and $\kappa_\mu \in [1.0, 2.5]$) are marked for further analyses of the regenerative and frictional chatters.

2. Grinding stability

With the model of the grinding process, the linear grinding stability can be studied by eigenvalue analysis. Before that, Eq. (2) is nondimensionlized by introducing the following dimensionless parameters

$$\begin{aligned}
&\xi_g = \frac{c_g}{\sqrt{m_g k_g}}, \quad \xi_w = \frac{c_w\sqrt{m_g}}{m_g\sqrt{k_g}}, \quad \xi_t = \frac{c_w\sqrt{m_g}}{J_t\sqrt{k_g}}, \quad \kappa_\mu = \frac{k\mu}{k_g}\left(R_g + R_d\right)^{\mu-1}, \quad \kappa_w = \frac{k_w m_g}{k_g m_w}, \quad \kappa_t = \frac{k_t m_g}{J_t k_g},\\
&\gamma_t = \frac{m_g R_d(R_g + R_d)}{J_t}, \quad \gamma_w = \frac{m_g}{w}, \quad \nu = \frac{f}{R_d + R_g}, \quad r_d = \frac{R_d}{R_d + R_g}, \quad r_g = \frac{R_d}{R_g + R_g}, \quad p = \frac{P}{L},\\
&\omega_w = \Omega_w\sqrt{\frac{m_g}{k_g}}, \quad \omega_g = \Omega_g\sqrt{\frac{m_g}{k_g}}, \quad e = 2\frac{m_d}{m_w}e_d, \quad \tau_w = T_w\sqrt{\frac{k_g}{m_g}}, \quad \tau_g = T_g\sqrt{\frac{k_g}{m_g}},
\end{aligned} \tag{9}$$

and variables

$$\begin{aligned}
&\tau = t\sqrt{\tfrac{k_g}{m_g}}, \quad x_g(\tau) = \tfrac{X_g(t)}{R_g+R_d}, \quad x_p(\tau) = \tfrac{X_p(t)}{R_g+R_d}, \quad y_p(\tau) = \tfrac{Y_p(t)}{R_g+R_d}, \quad \gamma(\tau) = \tan^{-1}\left(\tfrac{y_p(\tau)}{1-\nu-x_p(\tau)+x_g(\tau)}\right),\\
&d_g = \Big(\nu + x_p(\tau) - x_g(\tau)\Big)\cos\left(\gamma(\tau)\right) - y_p(\tau)\sin\left(\gamma(\tau)\right) - \Big(x_p(\tau-\tau_w) - x_g(\tau-\tau_w)\Big)\cos\left(\gamma(\tau-\tau_w)\right)\\
&\quad + y_p(\tau-\tau_w)\sin\left(\gamma(\tau-\tau_w)\right) - g\Big(x_p(\tau-\tau_g) - x_g(\tau-\tau_g)\Big)\cos\Big(\gamma(\tau-\tau_g)\Big) + g y_p(\tau-\tau_g)\sin\Big(\gamma(\tau-\tau_g)\Big).\\
&v_f = \omega_g r_g - \omega_w r_d - \dot\theta_p(\tau) r_d + \dot y_p(\tau)\cos\left(\gamma(\tau)\right) - \Big(\dot x_g(\tau) - \dot x_p(\tau)\Big)\sin\left(\gamma(\tau)\right).
\end{aligned} \tag{10}$$

Omitting mass eccentricity ($e = 0$) and linearising Eq. (2) with considering Eqs (9) and (10), one can study linear grinding stability with eigenvalue analysis and continuation scheme[2,15]. To begin with, the parameter values are

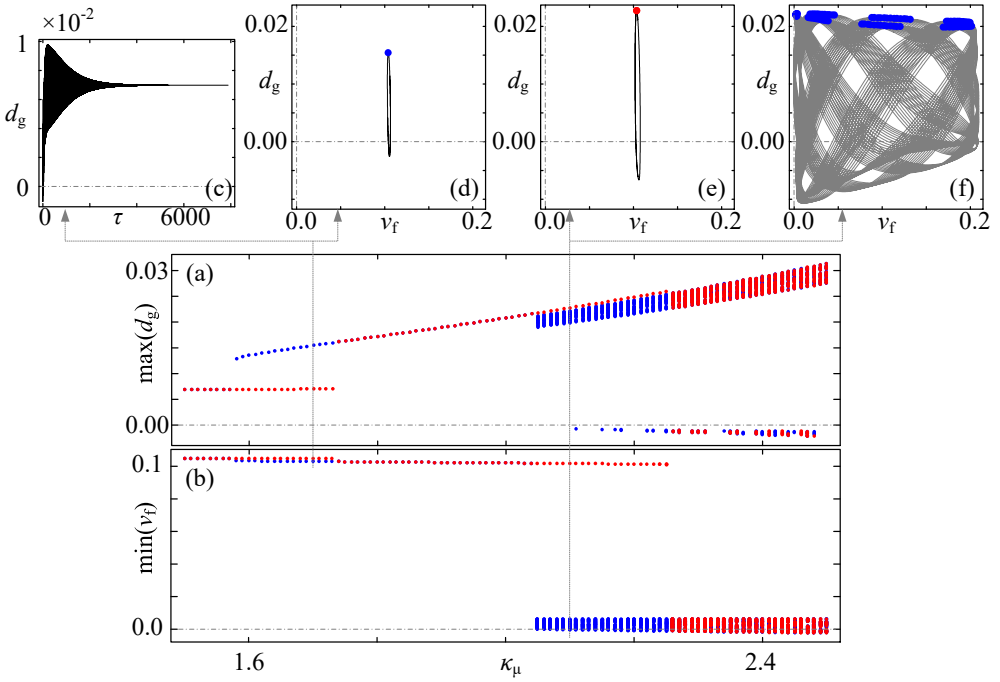

Fig. 4. Bifurcation diagrams on Arrow I, where (a) maximum d_g value and (b) minimum v_f value are plotted as functions of κ_μ. Here, results of forward and backward simulations are in red and blue dots, respectively. In addition, coexisting (c) stable grinding and (d) regenerative chatter for $\kappa_\mu = 1.43$ are displayed, while coexistence of (e) periodic regenerative and (f) quasi-periodic chatters for $\kappa_\mu = 2.1$ is depicted as well

selected as

$$\begin{aligned} &L = 1\ [\mathrm{m}], \quad R_w = 0.1\ [\mathrm{m}], \quad R_d = 0.25\ [\mathrm{m}], \quad R_g = 0.25\ [\mathrm{m}], \quad W = 0.03\ [\mathrm{m}], \\ &m_g = 20\ [\mathrm{kg}], \quad \rho = 7850\ [\mathrm{kg\ m^{-3}}], \quad c_g = 2\times10^5[\mathrm{N\ s\ m^{-1}}] \quad c_w = 1.2\times10^6[\mathrm{N\ s\ m^{-2}}], \\ &c_t = 822[\mathrm{N\ m\ s\ rad^{-1}}], \quad k_g = 3\times10^8[\mathrm{N\ m^{-1}}], \quad E = 2.06\times10^{11}[\mathrm{Pa}], \quad G = 7.93\times10^{10}[\mathrm{Pa}]. \end{aligned} \tag{11}$$

Corresponding results are depicted in Fig. 3 to illustrate the boundaries for both regenerative (black) and frictional (red) instabilities, which divide the planes into grey (stable) and white (unstable) regions. As seen, a small grinding stiffness κ_μ and a large delay τ_{w0} are wanted to maintain the linear stability. When the nominal depth ν is increased from 0.002 to 0.006, the black curves move downwards but the red ones upwards, which indicates that the regenerative stability is enhanced but the frictional one is impaired by deep grinding. When p increases from 0.1 to 0.9, corresponding to the wheel moving from the head to the tail of the workpiece, the black regenerative 'lobes' are flattened and the red frictional boundaries are unchanged. Next, to demonstrate the grinding chatters near different boundaries, Arrows I and II are marked for further bifurcation analyses.

3. Regenerative and frictional grinding chatters

On Arrow I, the stable and unstable regions are separated by the black boundary, corresponding with the regenerative instability. Performing numerical simulations and bifurcation analyses yields Figs 4(a) and (b), where maximum d_g and minimum v_f are plotted as functions of κ_μ. Results of forward (κ_μ increases from 1.5 to 2.5) and backward (κ_μ decrease from 2.5 to 1.5) simulations are represented by red and blue dots, respectively.

It is seen that the grinding is linearly stable for $\kappa_\mu < 1.74$, where it encounters the regenerative boundary and incurs a subcritical Hopf bifurcation. This introduces a coexistence of the stable grinding and the regenerative chatter for $\kappa_\mu \in [1.58, 1.73]$. When κ_μ increases further, there only exists the periodic chatter until κ_μ reaches 2.05, where the frictional instability is involved to introduce another quasi-periodic chatter coexisting with the periodic one. The

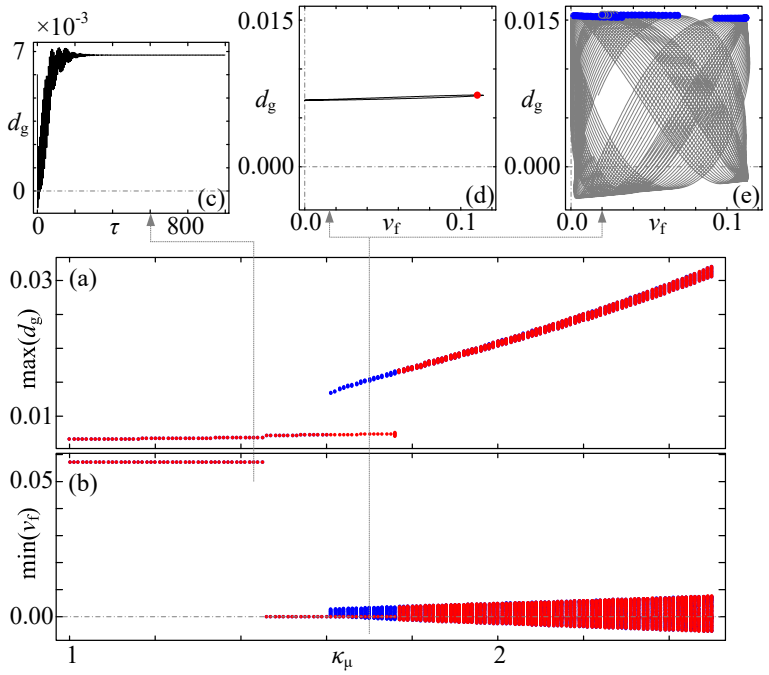

Fig. 5. Bifurcation diagrams on Arrow II, where (a) maximum d_g value and (b) minimum v_f value are plotted as functions of κ_μ. Here, results of forward and backward simulations are in red and blue dots, respectively. In addition, (c) the stable grinding for $\kappa_\mu = 1.43$, and coexistence of (d) the periodic frictional and (e) quasi-periodic chatters for $\kappa_\mu = 1.7$ are displayed.

periodic motion disappears for $\kappa_\mu > 2.25$, leaving only the quasi-periodic. To illustrate, phase portraits for the stable grinding and the regenerative chatter for $\kappa_\mu = 1.7$ and the periodic and quasi-periodic chatters for $\kappa_\mu = 2.1$ are displayed in Figs 4(c), (d), (e) and (b), respectively. In general, the chatter amplitude grows with respect to the increase of κ_μ, and the regenerative and frictional stabilities introduce the fluctuations of d_g and v_f, respectively.

Next, the bifurcation pattern on Arrow II is depicted in Fig. 5, which is dominated by the frictional instability. The grinding is stable for $\kappa_\mu < 1.46$, where the grinding jumps to a frictional chatter with large fluctuation of v_f but small variation of d_g. For κ_μ increasing further, the periodic frictional motion is unique before 1.61 is reached, where another quasi-periodic is introduced to coexist for $\kappa_\mu \in [1.61, 1.76]$. To illustrate, the stable grinding for $\kappa_\mu = 1.43$ and the periodic frictional and quasi-periodic chatters for $\kappa_\mu = 1.7$ are plotted in Figs 5(c), (d) and (e), respectively. Compared with the regenerative one, it is seen that the frictional instability does not induce any grinding chatter coexisting in the linearly stable region.

4. Chatters with workpiece imbalance

Then, the influence of workpiece imbalance (e=0.05) on the grinding chatters are discussed, which involves both the internal and external sources of instability. In this case, the workpiece can be regarded as a Jeffcott rotor[16,17]. With respect to Arrow I, the bifurcation pattern in Fig. 4 is transformed into that in Fig. 6. As seen, the bi-stability for $\kappa_\mu \in [2.05, 2.25]$ disappears, leaving a unique quasi-periodic chatter without frictional instability[2]. Besides, in the vicinity of the Hopf bifurcation point ($\kappa_\mu = 1.74$), the system shows a 'random' selection between the forced periodic vibration and quasi-periodic regenerative chatter. This phenomenon is similar to the result in our previous work[18], which has proved that the regenerative chatter can be quenched by artificially introduced sinusoid excitation. To illustrate, a small-amplitude forced vibration for $\kappa_\mu = 1.65$, and forced quasi-periodic regenerative chatter for $\kappa_\mu = 1.66$ and 2.1 are depicted in Figs 6(c), (d) and (e), respectively.

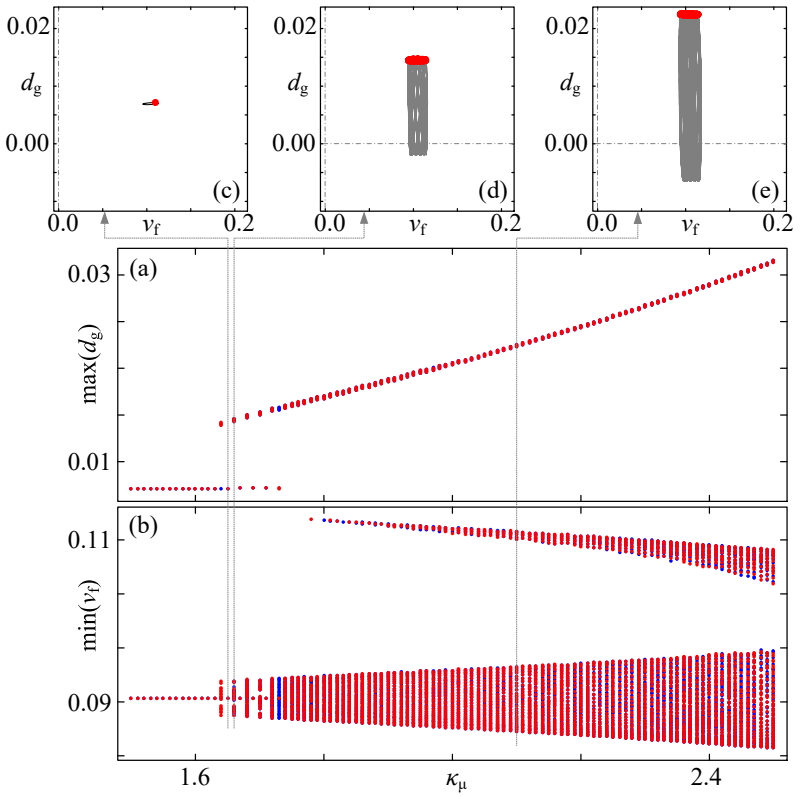

Fig. 6. Bifurcation diagrams on Arrow I, where (a) maximum d_g value and (b) minimum v_f value are plotted as functions of κ_μ. Results of forward and backward simulations are in red and blue dots, respectively. In addition, (c) the forced periodic vibration for $\kappa_\mu = 1.65$ and (d-e) the quasi-periodic regenerative chatter for $\kappa_\mu = 1.66$ and 2.1 are displayed.

With the workpiece imbalance, the corresponding bifurcation pattern on Arrow II is presented in Fig. 7. It is seen that the frictional chatter for $\kappa_\mu \in [1.46, 1.76]$ is quenched, and the afterwards quasi-periodic chatter is of no frictional instability (no stick motion). To illustrate, a forced periodic chatter for $\kappa_\mu = 1.43$ and a quasi-periodic regenerative one for $\kappa_\mu = 1.7$ are displayed in Figs 7(c) and (d), respectively.

5. Conclusions

Given internal (regeneration and friction) and external (workpiece imbalance), various grinding chatters involving planar and torsional movements were discussed. Eigenvalue analysis reveal the linear stability of the process, showing that a large grinding stiffness and a slow rotational workpiece speed benefit the stability. For a deep grinding, the regenerative stability is enhanced but the frictional one is impaired. Further bifurcation analysis demonstrate that the regenerative instability is subcritical, introducing a large-amplitude chatter coexisting with the stable grinding. By contrast, the frictional chatter exists only in the linearly unstable region, which emerges suddenly to replace the stable grinding. When the workpiece imbalance is involved, bifurcation analyses illustrate that the frictional instability is always quenched. By contrast, the regenerative chatter persists and is perturbed to be quasi-periodic.

Acknowledgements

This research is supported by National Natural Science Foundation of China under Grant No.11502048 and 11572224, and Fundamental Research Funds for the Central Universities under Grant No.ZYGX2015KYQD033.

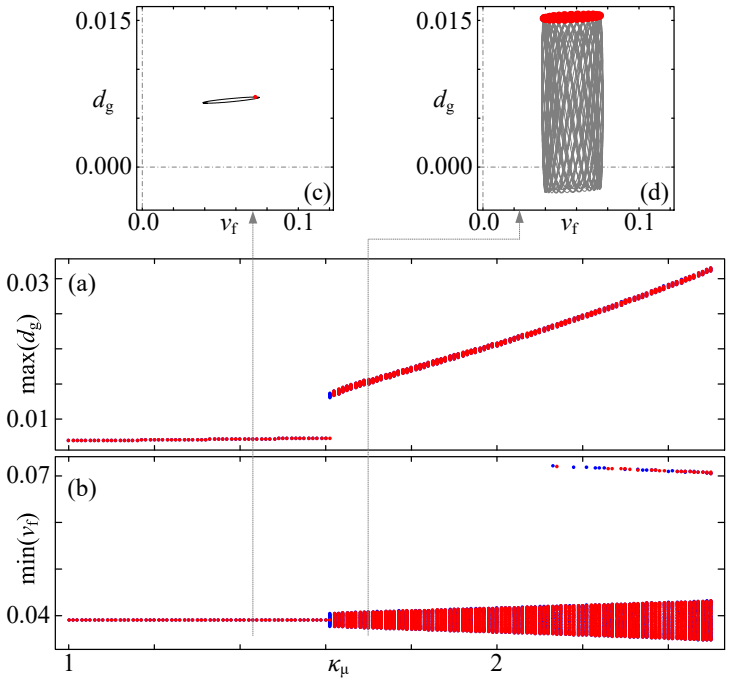

Fig. 7. Bifurcation diagrams on Arrow II, where (a) maximum d_g value and (b) minimum v_f value are plotted as functions of κ_μ. Results of forward and backward simulations are in red and blue dots, respectively. In addition, (c) the forced periodic vibration for $\kappa_\mu = 1.43$ and (d) the quasi-periodic regenerative chatter for $\kappa_\mu = 1.7$ and 2.1 are displayed.

References

1. Y. Altintas, M. Weck. Chatter stability of metal cutting and grinding. *CIRP ANN-MANUF TECHN* 2004;**53**(2):619-642.
2. Yao Yan, Jian Xu, Marian Wiercigroch. Regenerative and frictional chatter in plunge grinding. *Nonlinear Dyn* 2016;**86**:283-307.
3. Yao Yan, Jian Xu, Wanyong Wang. Nonlinear chatter witn large amplitude in a cylindrical plunge grinding process. *Nonlinear Dyn* 2012;**69**:1781-1793.
4. G. Werner. Influence of work material on grinding forces. *CIRP ANN-MANUF TECHN* 1978;**27**(1):243-248.
5. Jeehyun Jung, Pilkee Kim, Hyeonjun Kim, Jongwon Seok. Dynamic modeling and simulation of a nonlinear, non-autonomous grinding system considering spatially periodic waviness on workpiece surface. *SIMUL MODEL PRACT TH* 2015;**57**:88-99.
6. Yang Liu, Ekaterina Pavlovskaia, David Hendry, Marian Wiercigroch. Vibro-impact responses of capsule system with various friction models. *INT J MECH SCI* 2013;**72**:39-54.
7. R.N. Arnold. The mechanism of tool vibration in the cutting of steel. *Proceeding of the institution of mechanical engineers* 1946;**154**: 261-284.
8. R.A. Thompson. On the doubly regenerative stability of a grinder: the mathematica analysis of chatter growth. *J ENG IND* 1986;**108**: 83-92.
9. Kwok-wai Chung, Zhaoheng Liu. Nonlinear analysis of chatter vibration in a cylindrical transverse grinding process with two time delays usinganonlinear time transformation method. *Nonlinear Dyn* 2011;**66**(4): 441-456.
10. Dániel Bachrathy, Gábor Stépán, János Turi. State dependent regenerative effect in milling processes *J COMPUT NONLIN DYN* 2011;**6**(4):041002.
11. Tamás Insperger, David A.W. Barton, Gábor Stépán. Criticality of Hopf bifurcation in state-dependent delay model of turning processes. *INT J NONLIN MECH* 2008;**43**: 140-149.
12. Xianbo Liu, Nicholas Vlajic, Xinhua Long, Guang Meng, Balakumar Balachandran. Coupled axial-torsional dynamics in rotary drilling with state-dependent delay: stability and control. *Nonlinear Dyn* 2014;**78**:1891-1906.
13. Stephen Malkin, Changsheng Guo. *Grinding Technology*. 2nd ed. New York: Industrial Press; 2008.
14. Yao Yan, Jian Xu, Marian Wiercigroch. Regenerative chatter in self-interrupted plunge grinding. *Meccanica* 2016;**51**:3185-3202.
15. Zhaoheng Liu, Guy Payre. Stability analysis of doubly regenerative cylindrical grinding process. *J SOUND VIB* 2007;**301**:950-962.
16. H.H. Jeffcott. The lateral vibration of loaded shafts in the neighbourhood of a whirling speed - the effect of want of balance. *Philos Mag Series 6* 1919;**37**(219):304-314.
17. E.V. Karpenko, E.E. Pavlovskaia, M. Wiercigroch. Bifurcation analysis of a preloaded Jeffcott rotor. *CHAOS SOLITON FRACT* 2003;**15**(2):407-416.
18. Yao Yan, Jian Xu, Marian Wiercigroch. Non-linear analysis and quench control of chatter in plunge grinding. *INT J NONLIN MECH* 2016;**70**:134-144.